RMn_6Sn_6 compounds (R=Mg, Zr, and Hf) studied by ^{119}Sn Mössbauer spectroscopy and band structure calculations

T. Mazet,[1,*] J. Tobola[1,2] G. Venturini,[1] and B. Malaman[1]

[1]*Laboratoire de Chimie du Solide Minéral, Université Henri Poincaré-Nancy I, Associé au CNRS (UMR 7555), B.P. 239, 54506 Vandoeuvre-les-Nancy Cedex, France*

[2]*Faculty of Physics and Nuclear Techniques, University of Mining and Metallurgy, Al. Mickiewicza 30, 30-059 Cracow, Poland*

(Received 12 July 2001; published 7 February 2002)

The RMn_6Sn_6 compounds (R=Mg, Zr, and Hf) of $HfFe_6Ge_6$-type structure were investigated by ^{119}Sn Mössbauer spectroscopy and first-principles electronic structure calculations based on the Korringa-Kohn-Rostoker method in a nonrelativistic approach. The purpose of this study was to gain information on the electronic and magnetic properties of these materials with an emphasis on the hyperfine fields *transferred* on the nucleus of the three crystallographically inequivalent tin atoms. These huge hyperfine fields (as large as 33 T) are found to be independent of the R metal valence. The calculations indicate that the hyperfine fields are negative (with respect to the Mn magnetic moment) and good agreement with experiment is found. The chemical bonding is discussed based on the *l*-decomposed site projected densities of states. The theoretical results also provide interesting predictions to be confirmed by future transport and photoemission experiments.

DOI: 10.1103/PhysRevB.65.104406 PACS number(s): 71.20.Lp

I. INTRODUCTION

The RMn_6Sn_6 compounds crystallize in the $HfFe_6Ge_6$-type structure ($P6/mmm$). Interestingly, in this relatively simple cell, tin atoms occupy three inequivalent crystallographic positions. The compounds involving a nonmagnetic R element (R=Mg, Sc, Y, Lu, Zr, and Hf) are known to exhibit magnetic properties which depend significantly on the valence of the R metal.[1–3] Indeed, according to neutron diffraction experiments, three kinds of magnetic arrangements have been found: $MgMn_6Sn_6$ is ferromagnetic, and RMn_6Sn_6 compounds with a trivalent R metal (R=Sc, Y, and Lu) show helimagnetic order, while RMn_6Sn_6 compounds involving a tetravalent R atom (R=Zr and Hf) are essentially antiferromagnetic. This evolution of the magnetic arrangement is accompanied by a strong increase of the ordering temperatures, from T_c=290 K (R=Mg) up to $T_N \approx 580$ K for the tetravalent R compounds. All these magnetic structures are built upon ferromagnetic (001) Mn planes with the Mn moments in the basal plane and a saturated Mn moment value close to $\mu_{Mn} \approx 2.2\mu_B$ (see Sec. II for details).

^{119}Sn Mössbauer spectroscopy is a very efficient tool for probing the local environment of tin atoms. In magnetically ordered materials, the magnetic hyperfine interaction at the tin nuclei is related both to the magnetic arrangement of the magnetic sublattice and to the chemical bonding between tin atoms and these magnetic atoms. In the past, the occurrence of more or less large *transferred* hyperfine fields on the tin nuclei, sometimes partially or fully anisotropic, has been shown for numerous binary iron-tin or manganese-tin compounds,[4–9] some of them having a crystal structure closely related to the $HfFe_6Ge_6$ type. More recently, very large hyperfine fields (up to 33 T) have been found at the tin nuclei of RMn_6Sn_6 compounds involving trivalent R metals.[10,11] However, the experimental data, taken prior to neutron diffraction experiments, were misinterpreted since the authors concluded to an antiferromagnetic arrangement for the Mn moments in the (001) plane.

Furthermore, it is now well established that electronic structure calculations provide a reliable basis for the understanding of hyperfine magnetic interactions[12] by allowing a microscopic description of experimental facts often difficult to fully interpret since hyperfine interactions originate from the inner region of the atoms close to the nucleus.

It was thus decided to investigate both experimentally (by means of ^{119}Sn Mössbauer spectroscopy) and theoretically [using nonrelativistic Korringa-Kohn-Rostoker (KKR) band structure calculations] the *transferred* hyperfine fields acting on tin nuclei of recently stabilized RMn_6Sn_6 compounds (R=Mg, Zr, and Hf). Further, we also made use of our calculations to describe the electronic structure of these materials so as to gain a better understanding of some previous experimental results.

The organization of the paper is as follows. Section II presents the crystal and magnetic structures of the studied compounds. In Sec. III we discuss the different contributions to the total *transferred* hyperfine field at tin nuclei. Section IV deals with experimental and theoretical details. In Sec. V we present the results of ^{119}Sn Mössbauer experiments. Sec. VI gives the results for our calculations together with some comparisons to experimental data. Finally, the paper is summarized in Sec. VII.

A preliminary account of this work has been given in a conference paper.[13]

II. CRYSTAL AND MAGNETIC STRUCTURES

In the layered $HfFe_6Ge_6$-type RMn_6Sn_6 compounds (Fig. 1), the Mn atoms occupy the $6i$ site (1/2, 0, $z_{Mn} \approx 0.252$) and the R atoms enter the $1b$ site (0, 0, 1/2), while the Sn atoms are located on three different sites having axial local symme-

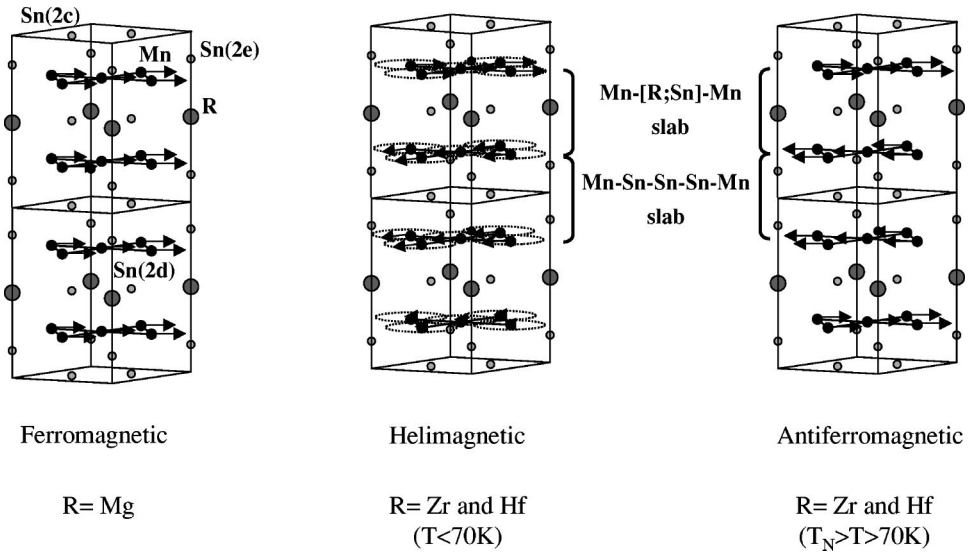

FIG. 1. Crystal and magnetic structures of $R\mathrm{Mn_6Sn_6}$.

try, namely, Sn($2c$) (1/3, 2/3, 0), Sn($2d$) (1/3, 2/3, 1/2), and Sn($2e$) (0, 0, $z_{Sn}\approx 0.17$). The Sn($2c$) and Sn($2d$) sites are situated in trigonal Mn prisms (Fig. 2) with three additional R atoms in the basal plane for Sn($2d$). Since $z_{Mn}>0.25$, the Mn-Sn($2c$) interatomic distance (≈ 2.75 Å) is slightly larger than the Mn-Sn($2d$) distance (≈ 2.72 Å). The Sn($2e$) atom is farther from the Mn atoms (≈ 2.80 Å) and it is slightly outside of the hexagonal Mn plane (kagomé net) with one R atom and one Sn($2e$) atom as next nearest neighbors along the c axis. Finally, it is worth noting that, despite similar atomic radii for magnesium, zirconium, and hafnium, $\mathrm{MgMn_6Sn_6}$ is found to crystallize with cell parameters ($a=5.517$ Å, $c=9.032$ Å) significantly larger than those of $\mathrm{ZrMn_6Sn_6}$ ($a=5.452$ Å, $c=8.978$ Å) and $\mathrm{HfMn_6Sn_6}$ ($a=5.442$ Å, $c=8.968$ Å).[2]

The $\mathrm{MgMn_6Sn_6}$ compound is ferromagnetic below $T_C=290$ K, while $\mathrm{ZrMn_6Sn_6}$ and $\mathrm{HfMn_6Sn_6}$ are antiferromagnetic below $T_N=580$ K and $T_N=575$ K, respectively. Previous neutron diffraction experiments[1–3] have shown that their magnetic structures (Fig. 1) may be described as an alternating stacking along the c axis of two different slabs built upon ferromagnetic easy-plane (001) Mn sheets: the ferromagnetic Mn-Sn($2e$)-Sn($2c$)-Sn($2e$)-Mn slab and the Mn-[R;Sn($2d$)]-Mn slab within which the Mn-Mn interlayer coupling is strongly dependent on both R valency and temperature. Indeed, for $R=$Mg the interlayer coupling is ferromagnetic, whereas it is antiferromagnetic above $T_t\approx 70$ K for $R=$Zr and Hf, leading to an antiferromagnetic structure ($+--+$) with the magnetic cell being twice the crystallographic cell along the c axis ($\mathbf{k}=\langle 0, 0, 1/2\rangle$). Below this temperature, $\mathrm{ZrMn_6Sn_6}$ and $\mathrm{HfMn_6Sn_6}$ present incommensurate helimagnetic arrangements ($\mathbf{k}=\langle 0, 0, q_z\rangle$) with a weakly temperature-dependent q_z component. At $T=2$ K, $q_z\approx 0.485$ and the Mn-Mn coupling through the Mn-[R;Sn($2d$)]−Mn slab deviates by approximately 10° from perfect antiferromagnetic alignment. Note that no change in the magnitude of the ordered magnetic moment is observed at the commensurate-incommensurate transition. Furthermore, unlike the ordering temperatures, the magnitude of the magnetic moment carried by Mn atoms is found to be nearly independent of the valence of the R metal ($\mu_{Mn}\approx 2.2\mu_B$ at 2 K).

III. ORIGIN OF THE HYPERFINE FIELD AT THE Sn NUCLEI

The hyperfine field (H_{hf}) acting on the nuclei of the nominally diamagnetic tin atoms, in the magnetically ordered state of $R\mathrm{Mn_6Sn_6}$, arises essentially from the hybridization between the sp valence states of tin and the self-polarized d states of manganese atoms.

The total hyperfine field at the tin nuclei is the sum of three different contributions: namely, the Fermi contact term and the dipolar and orbital fields.

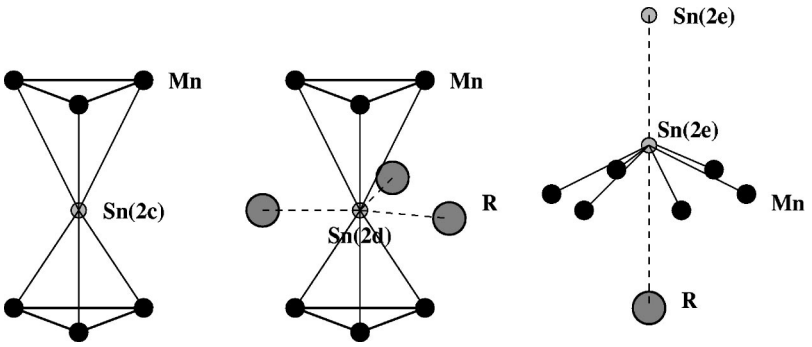

FIG. 2. Atomic environment of the inequivalent crystallographic Sn sites of the $R\mathrm{Mn_6Sn_6}$ compounds.

Generally, the Fermi contact interaction is the dominating contribution. It arises from the finite spin density of $5s$ electrons at Sn nuclei and, in the nonrelativistic limit, is given by the general formula[17]

$$H_{Fermi}=\frac{8}{3}\pi\mu_B[\rho_\uparrow(0)-\rho_\downarrow(0)], \tag{3.1}$$

where $\rho_\uparrow(0)$ and $\rho_\downarrow(0)$ denote the spin-dependent electron densities at the point nucleus ($r=0$). The works of Kanamori *et al.*[14,15] and subsequent studies[16,17] have allowed explaining the systematic variation of impurity hyperfine fields in ferromagnetic $3d$ metals as a function of the atomic number of the impurity.[18] According to these studies, the hybridization between s states of the impurity with the spin-polarized d states of the host leads to bonding and antibonding states in the local s density of states (DOS) of the impurity. At the beginning of each row of the periodic table, only the bonding states are populated, which leads, in a similar way to the effect discussed by Daniel and Friedel,[19] to a negative polarization at the impurity site resulting in a negative hyperfine field. The increase to large positive hyperfine field values at the end of the period and the abrupt decrease to negative values at the beginning of the next period are due to the progressive filling of the spin-split antibonding states. Therefore, the sign and magnitude of the Fermi contact contribution to the total hyperfine field of an sp element are determined by competition between the negative contribution of the bonding states and the positive contribution of the antibonding states. This model has also been used to explain the hyperfine fields of sp impurities on Ni and Fe surfaces.[20]

The dipolar contribution may be viewed as the sum of a lattice contribution, due to the moments of neighboring atoms, and a local contribution arising from the nonspherical valence p spin density of tin resulting from the hybridization with the spin-polarized d states of transition metal. The lattice dipolar field is small (less than 1 T) while the local dipolar field can be as large as several teslas for Sn atoms.[7–9,21] The dipolar field is not necessarily collinear with the contact field.

Finally, because of the spin-orbit coupling, the spin polarization of Sn p states induces an orbital polarization which is responsible for the orbital hyperfine field. This valence orbital contribution has been evaluated using fully relativistic band structure calculations for $5d$ impurities dissolved in Fe.[22] The valence p orbital contribution has been found roughly constant all across the $5d$ series (≈ 5 T). The magnitude of this contribution has not been estimated for Sn atoms but is expected to be small.

Therefore, neglecting the orbital field and considering only the six nearest-neighbor Mn atoms of the Sn atom, the total *transferred* hyperfine field can be expressed by[7–9]

$$\vec{H_{hf}}=A_p\sum_{i=1}^{6}(\vec{\mu_i}\cdot\vec{u_i})\vec{u_i}-\frac{A_p}{3}\sum_{i=1}^{6}\vec{\mu_i}+A_s\sum_{i=1}^{6}\vec{\mu_i}, \tag{3.2}$$

where $\vec{u_i}$ is a unit vector directed along each Mn-Sn bond and $\vec{\mu_i}$ is the magnetic moment of the corresponding Mn atom. The first two terms of Eq. (3.2) are related to the dipolar part of the *transferred* field due to p electrons, assuming that they remain localized in each Mn-Sn bond. The last term corresponds to the isotropic contact field due to the s spin density at the tin nuclei. A_p and A_s are, respectively, the dipolar and contact fields due to a unit Mn magnetic moment.

In the $R\mathrm{Mn_6Sn_6}$ compounds, the (001) Mn planes are ferromagnetic. Consequently, because of the arrangement of the six first-neighbor Mn atoms around the Sn atom, it is obvious from Eq. (3.2) that the dipolar field is necessarily collinear with the isotropic field and cancels for Sn($2d$) in the high-temperature antiferromagnetic phase of $\mathrm{ZrMn_6Sn_6}$ and $\mathrm{HfMn_6Sn_6}$. Therefore, due to the lack of spin reorientation in the studied compounds, the ^{119}Sn Mössbauer experiments do not allow showing the occurrence of the dipolar field.

IV. EXPERIMENTAL AND COMPUTATIONAL DETAILS

The polycrystalline samples used for the ^{119}Sn Mössbauer spectroscopy experiments were those employed during previous neutron diffraction experiments.[2,3]

The ^{119}Sn resonance absorption measurements were carried out using a constant-acceleration spectrometer. The velocity scale was calibrated with a ^{57}CoRh source (25 mCi) and a metallic iron foil at room temperature. A $\mathrm{Ba}^{119m}\mathrm{SnO_3}$ source (10 mCi) kept at room temperature was used for ^{119}Sn measurements. In all cases, polycrystalline absorbers with natural abundance of the ^{119}Sn isotope and thickness of ≈ 15 mg/cm^2 were used. The measurements were performed between 300 K and 4.2 K in a liquid helium cryostat. A palladium foil of 0.5 mm thickness was used as a critical absorber for tin x rays.

The Mössbauer spectra were fitted with a least-squares method program[23] assuming Lorentzian peaks.

The nonrelativistic electronic structure calculations were carried out using the fully charge- and spin-self-consistent KKR method.[24,25] In the KKR method we have used, both core states and valence states are calculated self-consistently. The crystal potential of muffin-tin form was constructed within the local spin density framework using the exchange-correlation term of von Barth and Hedin.[26] The self-consistency cycles were repeated for each compound until the difference between the input and output potentials was ≈ 1 mRy. The low-temperature experimental values of the lattice parameters and the atomic coordinates deduced from the previous neutron diffraction refinements were used. An optimal filling factor of the Wigner-Seitz cell ($\approx 62\%$) was obtained using nonoverlapping muffin-tin spheres with radii close to 2.90 u.a., 2.55 u.a., and 2.60 u.a. for R, Mn, and Sn atoms, respectively. Note that for a given compound the Sn muffin-tin radii were chosen to be strictly equal for the three tin sites. For the final potentials, the total DOS and the site-decomposed DOS as well as the l-decomposed partial DOS (with $l_{max}=2$) were computed on a 601-energy-point mesh with a tetrahedral k-space integration technique using 192 small tetrahedra and 75 k points in the irreducible part of the Brillouin zone as described in Ref. 27. For more details about the KKR method, see Ref. 24.

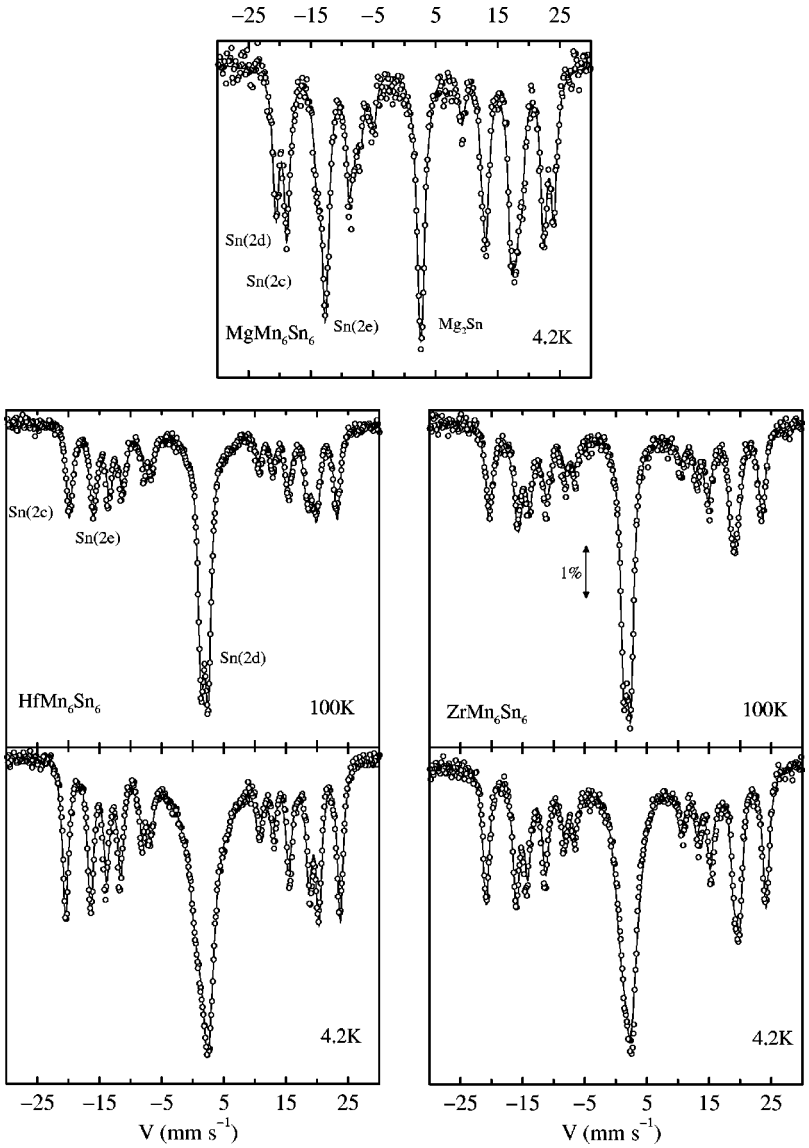

FIG. 3. ^{119}Sn Mössbauer spectra of $R\mathrm{Mn_6Sn_6}$ at 4.2 K and 100 K together with their least-squares envelopes.

V. ^{119}Sn MÖSSBAUER STUDY

A. Preliminary remarks

The quadrupole interaction reflects the asymmetry of charge distribution around the Sn nucleus. From the axial local symmetry at the three Sn sites, one expects $\eta=0$ with the principal Z axis of the electric field gradient (EFG) tensor along the c axis. In the Townes-Dailey approximation,[28] V_{ZZ} is proportional to $[(N_X+N_Y)/2-N_Z]$, where N_X, N_Y, and N_Z are related to the electronic populations of the $5p_X$, $5p_Y$, and $5p_Z$ orbitals, respectively. Considering the different environments of the three crystallographically inequivalent Sn sites (Fig. 2), the values of the EFG are related by $|V_{ZZ}^{(2c)}|>|V_{ZZ}^{(2d)}|>|V_{ZZ}^{(2e)}|$. Furthermore, for a magnetic site with axial symmetry, the apparent quadrupole splitting (2ϵ) is given, to first order, by

$$2\epsilon=\frac{eQV_{ZZ}}{2}\left(\frac{3\cos^2\theta-1}{2}\right)=\Delta\left(\frac{3\cos^2\theta-1}{2}\right), \quad (5.1)$$

where θ is the angle between the hyperfine field direction and the principal Z axis of the EFG tensor. Since in the $R\mathrm{Mn_6Sn_6}$ compounds (R=Mg, Zr, and Hf) the Mn magnetic moments are located in the basal plane, $\theta=90°$ and the attribution of the sites becomes obvious.

B. Results and interpretation

The ^{119}Sn Mössbauer spectra of $\mathrm{ZrMn_6Sn_6}$ and $\mathrm{HfMn_6Sn_6}$ recorded at 4.2 K and 100 K (above the commensurate-incommensurate transition temperature $T_t\approx 70$ K detected by neutron diffraction) are shown in Fig. 3 together with that of $\mathrm{MgMn_6Sn_6}$ obtained at 4.2 K. In all cases, the ^{119}Sn Mössbauer spectra are characteristic of tin nuclei experiencing large hyperfine fields and, as expected, three types of spectra are observed.

According to the ferromagnetic behavior of the $\mathrm{MgMn_6Sn_6}$ compound, the corresponding 4.2 K Mössbauer spectrum is characterized by three sextuplets. The strong central peak corresponds to the $\mathrm{Mg_2Sn}$ impurity previously detected in the neutron diffraction patterns.[3]

TABLE I. Hyperfine interaction parameters of ^{119}Sn in RMn_6Sn_6 compounds at the indicated temperatures. The Δ values given in parentheses were calculated using Eq. (5.1) from the fitted 2ϵ values. Otherwise, the sign of Δ is given only when it was established experimentally. The details are discussed in the text. For E_γ=23.875 keV the γ transition in ^{119}Sn: 1 mm s^{-1} corresponds to $7.963(2)\times10^{-8}$ eV or 19.253(6) MHz.

Compound	T (K)	Site	Γ (mm s^{-1}) ±0.06	IS (mm s^{-1}) ±0.08	2ϵ (mm s^{-1}) ±0.08	Δ (mm s^{-1}) ±0.08	H (T) ±0.3
$MgMn_6Sn_6$	4.2	$2e$	1.25	2.14	+0.04	(-0.08)	21.7
		$2d$	1.21	2.04	-0.68	(+1.36)	32.5
		$2c$	1.21	2.25	-1.00	(+2.00)	30.0
$ZrMn_6Sn_6$	100	$2e$	1.23	1.87	+0.00	(+0.00)	25.7
		$2d$	1.23	1.82		1.03	0
		$2c$	1.24	1.96	-0.77	(+1.54)	32.1
	4.2	$2e$	1.34	1.95	+0.01	(+0.02)	26.2
		$2d$	2.41	1.92		+0.88	1.2
		$2c$	1.29	2.03	-0.76	(+1.52)	32.9
$HfMn_6Sn_6$	100	$2e$	1.25	1.87	+0.00	(+0.00)	26.2
		$2d$	1.23	1.78		1.10	0
		$2c$	1.21	1.97	-0.80	(+1.60)	31.5
	4.2	$2e$	1.18	1.90	+0.01	(+0.02)	26.8
		$2d$	2.54	1.85		+0.95	1.5
		$2c$	1.17	2.02	-0.79	(+1.58)	32.3

As concerns $ZrMn_6Sn_6$ and $HfMn_6Sn_6$, the appearance of a quadrupole doublet for Sn($2d$) above T_t corresponds to the antiferromagnetic neighborhood of this site deduced from the neutron diffraction experiments.[2] Below T_t, this doublet broadens slightly due to a small *transferred* hyperfine field arising from the nonstrictly antiferromagnetic Mn-Mn alignment through the Mn-[R,Sn($2d$)]-Mn slab. Consequently, at the Sn($2d$) site, the quadrupole and magnetic interactions are of comparable magnitudes and it is therefore necessary to diagonalize the full hyperfine Hamiltonian (with $\eta=0$ and $\theta=90°$) to analyze the data. Attempts to fit this enlarged doublet with acceptable constrained values for the resonance widths ($\Gamma\approx0.9$–1.3 mm s^{-1}) were unsuccessful and led to the occurrence of external shoulders not observed on the experimental spectra. In a further step, we used unconstrained Γ values. This procedure resulted in rather good fits but with Γ values for Sn($2d$) twice those found for the two other Sn sites (Table I). This fit suggests that the hyperfine field values at Sn($2d$) are slightly spread out due to the presence of several helimagnetic phases ($\mathbf{k}_i=\langle 0,\ 0,\ q_{z_i}\rangle$). Since the q_z values must be very close, this phenomenon cannot be detected by powder neutron diffraction experiments. Nevertheless, similar behavior was previously observed for the R = Sc, Y, and Lu polycrystalline samples,[1] within which the q_{z_i} values were found to be more scattered.

For the title compounds, the isomer shift values are close to 2 mm s^{-1}. There is, however, a small increase of the charge density at the tin nucleus from the $2d$ site to the $2c$ site ($IS^{(2c)}>IS^{(2e)}>IS^{(2d)}$). The asymmetry of charge distribution is found to be slightly enhanced upon decreasing the R valency for the $2c$ and $2d$ sites (see Table I).

There is no apparent dependence of the large hyperfine field values (up to 33 T) on the R valency. On the other hand, the influence of the Mn-Sn distances appears for instance through the H_{hf} values obtained for $MgMn_6Sn_6$ since $H_{hf}^{(2d)}>H_{hf}^{(2c)}>H_{hf}^{(2e)}$.

VI. ELECTRONIC STRUCTURE CALCULATIONS

A. Non-spin-polarized calculations: Bonding in RMn_6Sn_6 systems

The total DOS and the site-projected l-decomposed DOS of $MgMn_6Sn_6$, $ZrMn_6Sn_6$, and $HfMn_6Sn_6$ are presented in Fig. 4.

As expected from the close chemical compositions, the electronic spectra are quite similar in all compounds. The total DOS is continuous over the whole energy range and is dominated by two peaks: the stronger one in the vicinity of the Fermi level (E_F) and the second one around 0.45 Ry. The main difference in the total DOS shape is observed above E_F where the sharp and relatively intense peaks seen for R = Zr and Hf nearly disappear in $MgMn_6Sn_6$.

At first glance, we observe that the electronic structure of the compounds results mainly from the d states of Mn and R (= Zr and Hf) atoms hybridized with the p states of Sn in the upper energy range while the lower-energy part is mostly constituted by the s states of Sn.

Considering the Mn states, the narrow peak at the Fermi energy is intense enough [$n^{Mn}(E_F)\approx60$ states/Ry] for the Stoner criterion $In(E_F)>1$ to be satisfied (from our spin-polarized calculations $I^{Mn}\approx0.03$ Ry). At zero temperature, the $In(E_F)$ product provides a criterion for the instability of

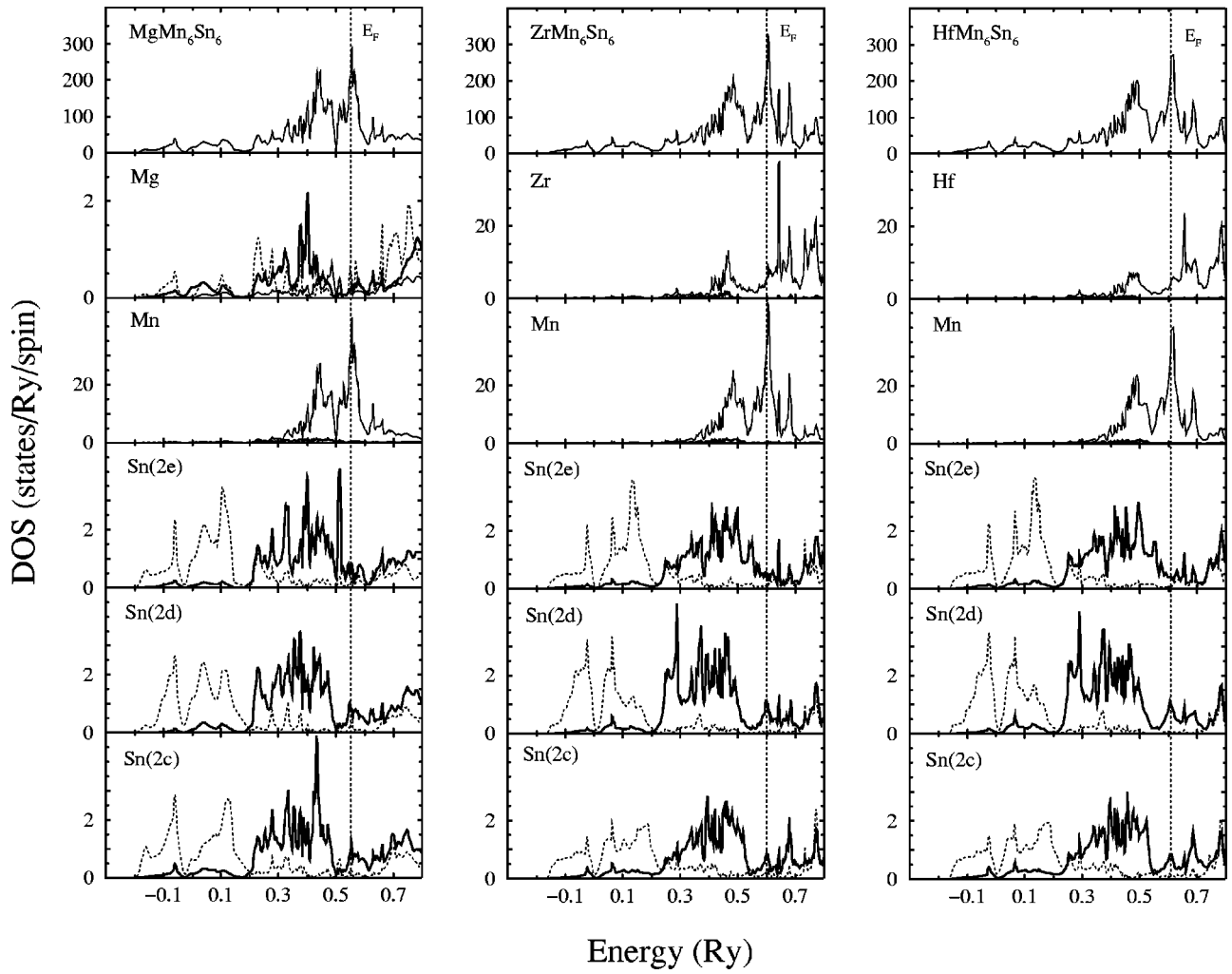

FIG. 4. KKR non-spin-polarized DOS for $MgMn_6Sn_6$, $ZrMn_6Sn_6$, and $HfMn_6Sn_6$. The upper panel is the total DOS. The lower panels show *l*-decomposed local DOS at the various inequivalent crystallographic sites. The *s*, *p*, and *d* contributions are plotted by dotted, solid thick, and solid thin lines, respectively. For the sake of clarity the *d* contributions on Sn sites are not shown. The Fermi level is marked by the dotted vertical line.

the nonmagnetic configuration towards intraband spin polarization.[29] Thus, in agreement with experimental results, magnetic properties in RMn_6Sn_6 are expected and spin-polarized calculations were undertaken (see Sec. VI B). It is worth noting that for other atoms (R and Sn) there is a low-density region around E_F. Therefore, the Mn *d* states confined in the large and narrow peak at E_F are essentially nonbonding, at least when dealing with Mn-R and Mn-Sn interactions.

The DOS on the Sn atoms is very similar whatever the Sn crystallographic site. Most of the *s* states are located in the lower-energy part (-0.2 Ry$<E<+0.2$ Ry) and, through hybridization, are responsible for the low-lying, barely visible, R and Mn densities of states. For higher energy we observe, however, small Sn *s* contributions hybridized with the Mn *d* states. The Sn *p* states are essentially found above 0.2 Ry. Hybridization between metalloid *p* states and transition-metal *d* states is known to lead to bonding and antibonding hybrids situated at the bottom and top of the transition-metal *d* band, respectively.[30,31] We conclude that the chemical bonding between the transition metal (Mn, Zr, and Hf) and the tin is mainly due to *d*-*p* hybridization, as generally observed in tin-based intermetallics.[33,34]

The origin of the main difference between the total DOS of $ZrMn_6Sn_6$ and $HfMn_6Sn_6$, on the one hand, and $MgMn_6Sn_6$, on the other hand, appears upon inspecting the R-DOS. Within the $R=$Zr and Hf muffin-tin spheres, the DOS is essentially of *d* symmetry and partly reflects that of the Mn atoms since the peaks centered around 0.45 Ry and above E_F are also present in the R *d*-DOS. We identify this ''two-peak'' structure as due to the bonding and antibonding states resulting from the hybridization between the Mn *d* states and the R (= Zr or Hf) *d* states. In the case of $MgMn_6Sn_6$, the DOS on the Mg site is less intense and comprises essentially *s* and *p* types, thus implying a different bonding with Mn atoms. It is well known that in metallic transition-element systems the largest contribution to cohesion is due to *d*-*d covalency*.[32] There is in addition relatively little interaction between the Mn *d* states and the less tightly bound magnesium valence levels. Consequently, the Mg-Mn

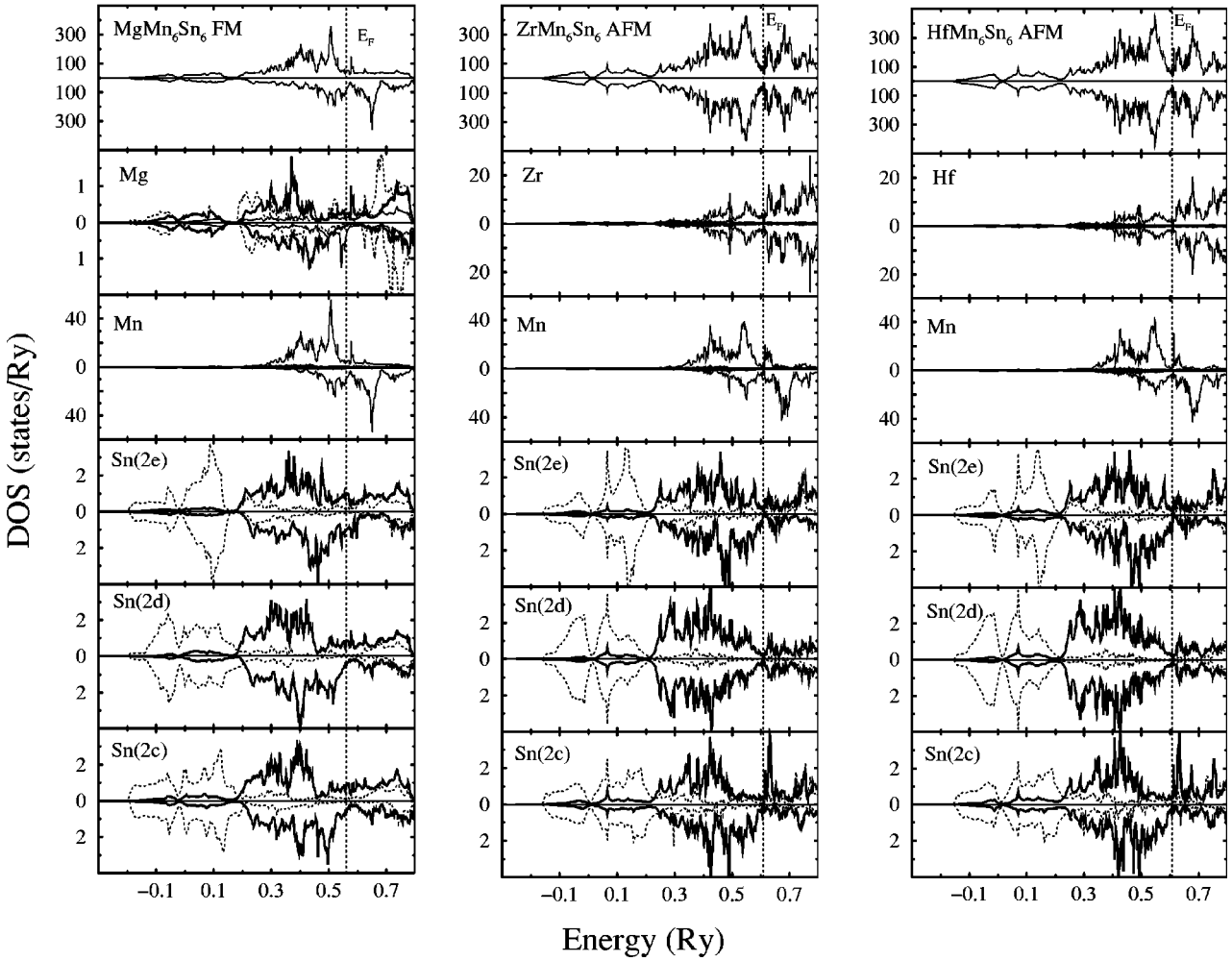

FIG. 5. KKR spin-polarized DOS for $MgMn_6Sn_6$, $ZrMn_6Sn_6$, and $HfMn_6Sn_6$. The upper panel is the total DOS. The lower panels show l-decomposed local DOS at the various inequivalent crystallographic sites. The s, p, and d contributions are plotted by dotted, solid thick, and solid thin lines, respectively. For the sake of clarity the d contributions on Sn sites are not shown. The Fermi level is marked by the dotted vertical line.

bond is weaker than the Zr-Mn or Hf-Mn bond. This can be related to the ''abnormally'' large cell parameters of $MgMn_6Sn_6$ with respect to those of $ZrMn_6Sn_6$ and $HfMn_6Sn_6$. This difference in the electronic structure could also explain the absence of $R_{1-x}R'_xMn_6Sn_6$ (R=Mg, R'=Zr or Hf) solid solutions.[2] Finally, we suggest that the modifications of the R-Mn bond play a determining role in the evolution of both the magnetic order and the ordering temperature with the R valency through indirect exchange interactions.

TABLE II. Calculated l-decomposed ($l_{max}=2$) and total magnetic moments in units of Bohr magnetons (μ_B) at the inequivalent crystallographic sites of the RMn_6Sn_6 compounds. The zero values at the R and Sn($2d$) sites in the antiferromagnetic $ZrMn_6Sn_6$ and $HfMn_6Sn_6$ phases are not indicated. The experimental Mn magnetic moment values were taken from Refs. 2 and 3.

	$MgMn_6Sn_6$					$ZrMn_6Sn_6$			$HfMn_6Sn_6$		
	Mn	Mg	Sn($2e$)	Sn($2d$)	Sn($2c$)	Mn	Sn($2e$)	Sn($2c$)	Mn	Sn($2e$)	Sn($2c$)
μ_s	0.009	-0.007	-0.014	-0.023	-0.022	0.008	-0.020	-0.023	0.008	-0.018	-0.022
μ_p	0.004	-0.030	-0.062	-0.071	-0.069	0.005	-0.062	-0.092	0.006	-0.062	-0.105
μ_d	2.207	-0.015	0.005	0.006	0.005	2.258	0.006	0.006	2.350	0.006	0.007
μ_{tot}	2.220	-0.052	-0.071	-0.088	-0.086	2.271	-0.076	-0.109	2.364	-0.074	-0.120
μ_{expt}	2.32					2.11			2.18		

TABLE III. Theoretical and experimental hyperfine field values (in units of T) at the Sn nuclei of the $R\mathrm{Mn_6Sn_6}$ compounds. All computed values are negative with respect to the magnetic moment of the first Mn neighbors (see text).

	$\mathrm{MgMn_6Sn_6}$			$\mathrm{ZrMn_6Sn_6}$			$\mathrm{HfMn_6Sn_6}$		
	Sn($2e$)	Sn($2d$)	Sn($2c$)	Sn($2e$)	Sn($2d$)	Sn($2c$)	Sn($2e$)	Sn($2d$)	Sn($2c$)
KKR	20.2	33.8	33.5	29.9	0	35.6	27.4	0	33.0
Expt.	21.7	32.5	30.0	26.2	0	32.9	26.8	0	32.3

B. Spin-polarized calculations: Local moments and Sn hyperfine fields

Since the spin-polarized KKR calculations refer to collinear spin arrangements, a pure antiferromagnetic $(+--+)$ arrangement was assumed for the $\mathrm{ZrMn_6Sn_6}$ and $\mathrm{HfMn_6Sn_6}$ systems, despite the fact that this magnetic structure is only stable for temperatures above $T_t \approx 70$ K. Such an approximation seems to be reasonable since the true helimagnetic low-temperature arrangement only slightly deviates from the aforementioned antiferromagnetic structure, as shown by the neutron diffraction[2] and the present ^{119}Sn Mössbauer experiments. Therefore, to allow for the magnetic symmetry in the case of $\mathrm{ZrMn_6Sn_6}$ and $\mathrm{HfMn_6Sn_6}$ we used a cell twice that of the chemical one by doubling of the c lattice constant (i.e., 26 atoms/cell).

The spin-polarized KKR computations of the $R\mathrm{Mn_6Sn_6}$ compounds, shown in Fig. 5, resulted in magnetic ground states which support experimental data.

By integrating the l-decomposed DOS up to the Fermi level we obtained the l contributions to local magnetic moments. As expected for Mn atoms, the moments mainly arise from polarizations of d states while s and p polarizations only add a small positive contribution. The calculated Mn magnetic moments are compared with neutron diffraction results in Table II.

Small magnetic moments are also found on other atoms because of the hybridization with the self-polarized d states of Mn atoms (Table II). In the ferromagnetic $\mathrm{MgMn_6Sn_6}$ compound, all sites [Sn($2e$), Sn($2d$), Sn($2c$), and Mg] present an imbalance in the population for the two spin channels. Conversely, the polarization of the R and Sn($2d$) sites, located within the antiferromagnetic Mn-[R,Sn($2d$)]-Mn slab, vanishes in $\mathrm{ZrMn_6Sn_6}$ and $\mathrm{HfMn_6Sn_6}$. These locally induced magnetic moments are negative, i.e., opposite to those of the first Mn neighbors.

The polarization of Sn electronic states is responsible for the hyperfine field at the tin nuclei measured by Mössbauer

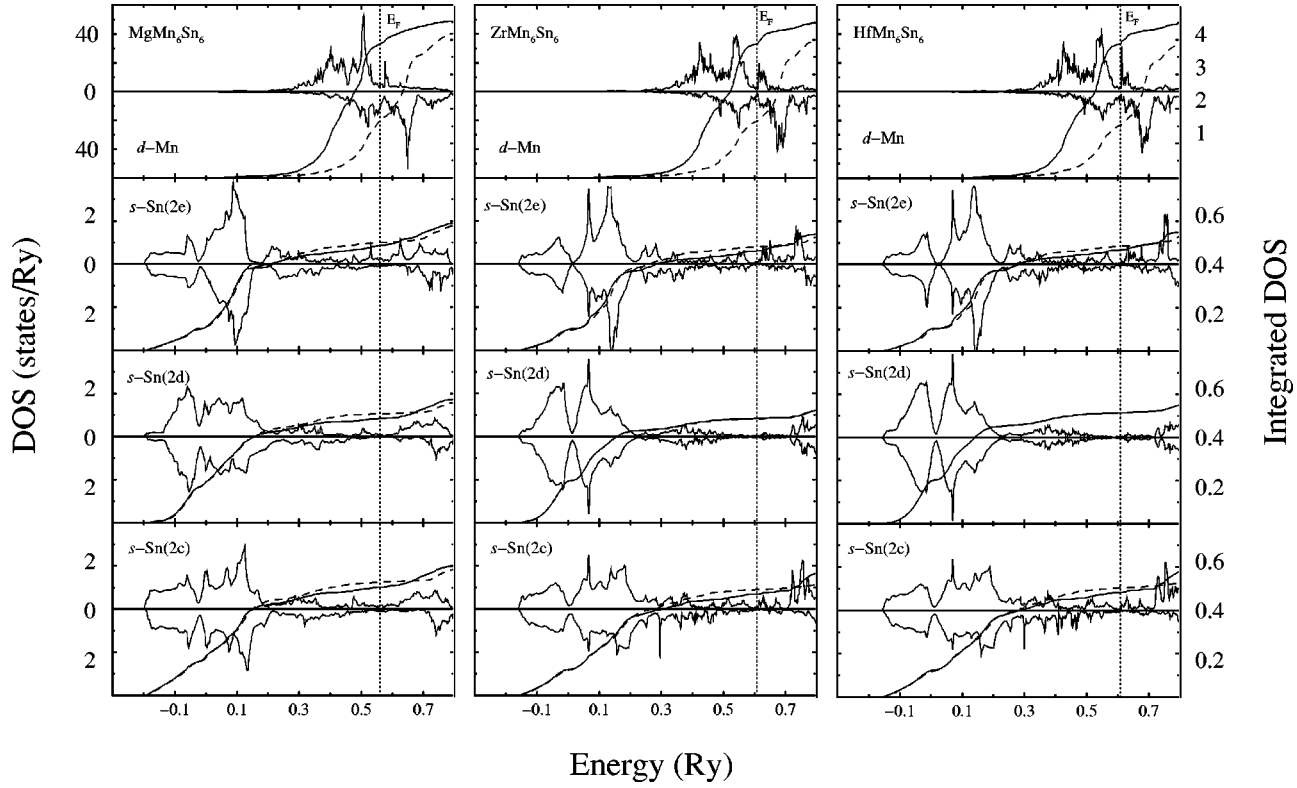

FIG. 6. Mn d-DOS (upper panel, left scale) and Sn s-DOS (lower panels, left scale) in $R\mathrm{Mn_6Sn_6}$ as well as the corresponding spin-resolved integrated l-like DOS (right scale). Solid and dashed lines correspond to spin-up and spin-down electrons, respectively. The Fermi level is marked by the dotted vertical line.

spectroscopy. The computed spin density at nuclear position allows us to determine, through Eq. (3.1), the Fermi contact contribution to the total hyperfine field which is related to the polarization of *s* symmetry electrons. Because of the approximations—the spherical shape of the potentials and the nonrelativistic treatment—the calculations do not allow computing, respectively, the dipolar and orbital contributions arising from polarized *p* states. The calculations show that the hyperfine fields are negative and, as expected for an *sp* element,[12] arise exclusively from valence electrons. The computed H_{hf} values are given in Table III and compared to Mössbauer spectroscopy data. The remarkable agreement between experimental and theoretical values, maybe a little fortuitous for R=Hf, suggests that the dipolar and orbital contributions to the total experimental hyperfine field are weak or cancel each other. Furthermore, by superposing the spin-resolved integrated DOS curves (Fig. 6), we clearly distinguish, for *s* symmetry states of the Sn atoms, two regions with different sign for the polarization: at low energy the polarization is negative and it changes sign at an energy above E_F. As explained by Kanamori *et al.*,[14,15] the low-energy part corresponds to the bonding states which show a preferential occupation for the minority spin states while the reverse is true for the antibonding states situated at higher energy. As found both experimentally and theoretically, the hyperfine field on the Sn($2e$) site is significantly smaller than those on Sn($2d$) and Sn($2c$) sites. This is due to the larger Mn-Sn distance for the former site and the resulting smaller bonding-antibonding splitting. This effect is conspicuous in Fig. 6, where one observes that the polarization changes sign at a lower energy for Sn($2e$) than for Sn($2d$) and Sn($2c$). In conclusion, the huge Sn hyperfine fields in RMn$_6$Sn$_6$ systems, to our knowledge the highest ever observed for Sn atoms, arise from the hybridization between the Mn 3*d* states and the Sn 5*s* states. Their very high negative magnitude is a consequence of the overall electronic structure of the RMn$_6$Sn$_6$ compounds: as shown by the corresponding integrated DOS (Fig. 6), the 5*s* states of Sn below the Fermi energy are strongly and negatively polarized; i.e., only the Sn 5*s*–Mn 3d bonding states are populated.

Interestingly, for ZrMn$_6$Sn$_6$ and HfMn$_6$Sn$_6$ (unlike MgMn$_6$Sn$_6$), the Fermi level E_F is observed in a deep minimum of the total DOS (Fig. 7), which suggests particular transport properties.

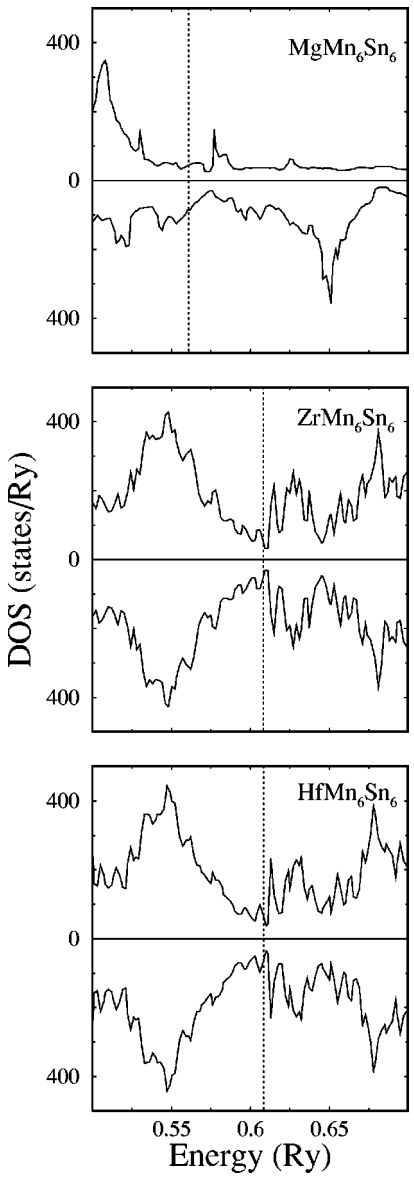

FIG. 7. Density of states in the vicinity of the Fermi level in the ferromagnetic MgMn$_6$Sn$_6$ and the antiferromagnetic ZrMn$_6$Sn$_6$ and HfMn$_6$Sn$_6$.

VII. SUMMARY

We have studied the RMn$_6$Sn$_6$ compounds (R=Mg, Zr, and Hf) by ^{119}Sn Mössbauer spectroscopy and band structure calculations using the KKR method.

The ^{119}Sn Mössbauer spectra are consistent with the magnetic structures inferred from previous neutron diffraction experiments. The amplitude of the very large *transferred* hyperfine fields (up to 33 T) at the ^{119}Sn nuclei is found to be independent of the valence of the *R* element, except through the evolution of the magnetic structures. The isomer shift values also do not alter significantly upon changing the *R* element while a small increase of the asymmetry of the charge distribution is observed when the valence of the *R* metal decreases.

The computed KKR values of the hyperfine fields at the Sn nuclei are very close to that found experimentally. The calculations show that these hyperfine fields are negative and stem exclusively from valence electrons. These large negative *transferred* hyperfine fields were successfully analyzed using the Kanamori model: in the RMn$_6$Sn$_6$ compounds, the Fermi level is situated in the region corresponding to the bonding states arising from the hybridization between Mn 3*d* states and Sn 5*s* states.

Finally, the electronic structure and chemical bonding of these materials were described. Remarkably, a very low density of states at the Fermi level was computed for the antiferromagnetic compounds involving a tetravalent *R* element (R=Zr and Hf). Photoemission experiments and electrical transport measurements are in progress.

We thank G. Le Caër for enlightening discussions.

*Corresponding author. Electronic address: thomas.mazet@lcsm.uhp-nancy.fr

[1] G. Venturini, D. Fruchart, and B. Malaman, J. Alloys Compd. **236**, 1629 (1996).
[2] T. Mazet, R. Welter, and B. Malaman, J. Alloys Compd. **284**, 54 (1999).
[3] T. Mazet, R. Welter, and B. Malaman, J. Magn. Magn. Mater. **204**, 11 (1999).
[4] G. Trumpy, E. Both, C. Djéga-Mariadassou, and P. Lecocq, Phys. Rev. B **2**, 3477 (1970).
[5] S. K. Kulshershtha and P. Raj, Solid State Commun. **28**, 787 (1978).
[6] G. Le Caër, B. Malaman, L. Häggström, and T. Ericsson, J. Phys. F: Met. Phys. **9**, 1905 (1979).
[7] G. Le Caër, B. Malaman, G. Venturini, and I. B. Kim, Phys. Rev. B **26**, 5085 (1982).
[8] G. Le Caër, B. Malaman, G. Venturini, D. Fruchart, and B. Roques, J. Phys. F: Met. Phys. **15**, 1813 (1985).
[9] G. Venturini, B. Malaman, G. Le Caër, and D. Fruchart, Phys. Rev. B **35**, 7038 (1987).
[10] Y. Amako, T. Yamamoto, and H. Nagai, Hyperfine Interact. **94**, 1897 (1994).
[11] Y. Amako, T. Yamamoto, M. Misawa, H. Yoshie, and H. Nagai, J. Magn. Magn. Mater. **140-144**, 1029 (1995).
[12] H. Akai, M. Akai, S. Blügel, B. Drittler, H. Ebert, K. Terakura, R. Zeller, and P. H. Dederichs, Suppl. Prog. Theor. Phys. **101**, 11 (1990) and references therein.
[13] T. Mazet, J. Tobola, G. Venturini, and B. Malaman, Acta Phys. Pol. A **97**, 737 (2000).
[14] J. Kanamori, H. Katayama-Yoshida, and K. Terakura, Hyperfine Interact. **8**, 573 (1981).
[15] J. Kanamori, H. Katayama-Yoshida, and K. Terakura, Hyperfine Interact. **9**, 363 (1981).
[16] M. Akai, H. Akai, and J. Kanamori, J. Phys. Soc. Jpn. **54**, 4246 (1985).
[17] S. Blügel, H. Akai, R. Zeller, and P. H. Dederichs, Phys. Rev. B **35**, 3271 (1987).
[18] G. N. Rao, Hyperfine Interact. **24-26**, 1119 (1985).
[19] E. Daniel and J. Friedel, J. Phys. Chem. Solids **24**, 1601 (1963).
[20] Ph. Mavropoulos, N. Stefanou, B. Nonas, R. Zeller, and P. H. Dederichs, Phys. Rev. Lett. **81**, 1505 (1998).
[21] J. P. Sanchez, P. Vulliet, M. M. Abd-Elmeguid, and D. Kaczorowski, Phys. Rev. B **62**, 3839 (2000).
[22] H. Ebert, R. Zeller, B. Drittler, and P. H. Dederichs, J. Appl. Phys. **67**, 4576 (1990).
[23] G. Le Caër (private communication).
[24] A. Bansil, S. Kaprzyk, P. E. Mijnarends, and J. Tobola, Phys. Rev. B **60**, 13 396 (1999) and references therein.
[25] S. Kaprzyk, Acta Phys. Pol. A **91**, 135 (1997).
[26] U. von Barth and L. Hedin, J. Phys. C **5**, 1629 (1972).
[27] S. Kaprzyk and P. E. Mijnarends, J. Phys. C **19**, 1629 (1972).
[28] C. H. Townes and B. P. Dailey, J. Chem. Phys. **17**, 782 (1949).
[29] J. F. Janak, Phys. Rev. B **16**, 255 (1977).
[30] P. S. Ho, G. W. Rubloff, J. E. Lewis, V. L. Moruzzi, and A. R. Williams, Phys. Rev. B **22**, 4784 (1980).
[31] C. D. Gelatt, Jr., A. R. Williams, and V. L. Moruzzi, Phys. Rev. B **27**, 2005 (1983).
[32] J. Kübler and V. Eyert, in *Materials Science and Technology: A Comprehensive Treatment*, edited by R. W. Cahn, P. Haasen, and E. J. Kramer (VCH, Weinheim, 1992), Vol. 3A, p. 1.
[33] S. F. Matar and V. Eyert, J. Magn. Magn. Mater. **166**, 321 (1997).
[34] S. F. Matar and A. Mavromaras, J. Solid State Chem. **149**, 449 (2000).